Something something something physics

Steven Green
of Emmanuel College

A dissertation submitted to the University of Cambridge
for the degree of Doctor of Philosophy

Abstract

This thesis describes the optimisation of the calorimeter design for collider experiments at the future Compact LInear Collider (CLIC) and the International Linear Collider (ILC). The detector design of these experiments is built around high-granularity Particle Flow Calorimetry that, in contrast to traditional calorimetry, uses the energy measurements for charged particles from the tracking detectors. This can only be realised if calorimetric energy deposits from charged particles can be separated from those of neutral particles. This is made possible with fine granularity calorimeters and sophisticated pattern recognition software, which is provided by the PandoraPFA algorithm. This thesis presents results on Particle Flow calorimetry performance for a number of detector configurations. To obtain these results a new calibration procedure was developed and applied to the detector simulation and reconstruction to ensure optimal performance was achieved for each detector configuration considered.

This thesis also describes the development of a software compensation technique that vastly improves the intrinsic energy resolution of a Particle Flow Calorimetry detector. This technique is implemented within the PandoraPFA framework and demonstrates the gains that can be made by fully exploiting the information provided by the fine granularity calorimeters envisaged at a future linear collider.

A study of the sensitivity of the CLIC experiment to anomalous gauge couplings that effect vector boson scattering processes is presented. These anomalous couplings provide insight into possible beyond standard model physics. This study, which utilises the excellent jet energy resolution from Particle Flow Calorimetry, was performed at centre-of-mass energies of 1.4 TeV and 3 TeV with integrated lumi-

nosities of 1.5ab^{-1} and 2ab^{-1} respectively. The precision achievable at CLIC is shown to be approximately one to two orders of magnitude better than that currently offered by the LHC.

Finally, a study into various technology options for the CLIC vertex detector is described.

Declaration

This dissertation is the result of my own work, except where explicit reference is made to the work of others, and has not been submitted for another qualification to this or any other university. This dissertation does not exceed the word limit for the respective Degree Committee.

Andy Buckley

Acknowledgements

Of the many people who deserve thanks, some are particularly prominent, such as my supervisor…

Preface

This thesis describes my research on various aspects of the LHCb particle physics program, centred around the LHCb detector and LHC accelerator at CERN in Geneva.

For this example, I'll just mention Chapter **??** and Chapter **??**.

Contents

"Writing in English is the most ingenious torture ever devised for sins committed in previous lives."

— James Joyce

Chapter 1

Capacitively Coupled Pixel Detectors for the CLIC Vertex Detector

"There, sir! that is the perfection of vessels!"
— Jules Verne, 1828–1905

1.1 Introduction

Successful identification of heavy-flavour quarks and tau-leptons relies upon precise reconstruction of the secondary displaced vertices produced in the decay of these particles as well as accurate association of the daughter tracks to those vertices. To achieve this for the CLIC experiment very high spatial resolution, of approximately 3 μm and good geometric coverage extending to low θ values are essential. The vertex detector must also have a low material budget, less than 0.2 X_0 per layer, as to not impact the performance of the other sub detectors and a low occupancy, aided by time-tagging to an accuracy of 10 ns, to counteract the high beam-induced backgrounds found near the impact point.

There are no commercially available technology options that fulfil all the criteria for the vertex detector, which had led the CLIC experiment to consider a variety of new technology options. The focus of this chapter is the use of high voltage complementary metal-oxide-semiconductor (HV-CMOS) active sensors coupled to a separate readout ASIC for the CLIC vertex detector.

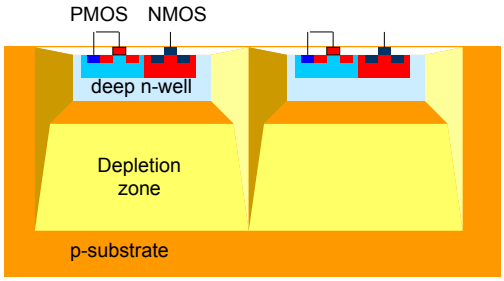

Figure 1.1: HV-CMOS diagram.

1.1.1 HV-CMOS

There are two classifications for pixel detectors; hybrid detectors where a passive sensor is bump-bonded to a separate readout chip and fully integrated where the collection diode is built upon the same wafer as the readout circuitry. Both of these technology options find the CLIC experimental conditions extremely challenging. Hybrid technologies struggle to achieved both the radiation tolerance and the functionality in the readout circuitry, while fully integrated circuits have too slow readout times due to limitations on the applied bias voltage.

HV-CMOS is adapted to the CLIC experimental conditions as the n-MOS and p-MOS transistors forming the integrated amplifier (or generic in-pixel logic operations in general) for collecting the signal are embedded within a deep n-well, as shown in figure 1.1. This acts as both the collection diode as well as providing shielding to the circuitry from the beam induced radiation. With the integrated circuitry shielded from the p-substrate it becomes possible to apply a large bias voltage to the substrate to widen the depletion region meaning that the main part of any signal deposited in the detector will be transferred via drift as opposed to diffusion, which provides the fast readout times required by the CLIC experiment.

HV-CMOS devices are strong candidates for the CLIC vertex detector, however, they do have limitations such as noise from interference between the n and p doped wells of the n-MOS and p-MOS transistors that sit within the deep n well. This noise will grow with the number of n-MOS and p-MOS devices on the wafer and so ultimately restricts the complexity of the in-pixel operations that can be performed. There are also topological difficulties such as the difficulty of applying the CMOS

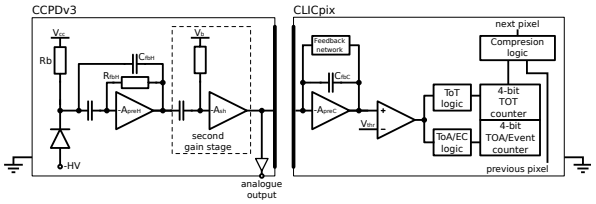

Figure 1.2: Schematic of CCPDv3 and CLICpix pixels.

process to all sizes and the fact that the deep n well does not occupy the full space of the pixel.

To minimise the material budget for the vertex detector, the pixels used are designed to be as thin as possible. This means the signal from the HV-CMOS will be small as the depletion region will be thin. To counter this, in-pixel signal amplification was applied to the HV-CMOS devices, as shown in figure 1.2. This increases the signal going to the readout ASIC, which also counteracts the intrinsically small capacitance between the HV-CMOS and readout ASIC.

1.1.2 CLICpix

The readout ASIC in this study is the CLICpix, which is a charge integrating amplifier connected to a discriminator as shown in figure 1.2. The output to this discriminator is then used as the input for further logic operations that record the magnitude, using a Time over Threshold (ToT) measurement, and time of arrival of the collected charge.

1.1.3 Capacitive Coupling

Solder bump-bonding is the typical method that is used for connecting active pixel sensors to the readout ASIC, however, the solder adds to the thickness of the sensor significantly as well as raising the cost. A viable alternative to this procedure is the replacement of the bump-bonding with a thin uniform layer of glue that forms a capacitive connection between the active pixel and readout ASIC. The mechanical tolerances on the alignment of the active pixel sensor and readout ASIC when applying this glueing procedure are the focus of this study.

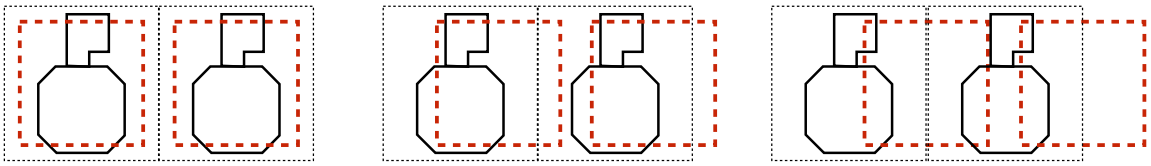

Figure 1.3: Schematic of alignment of CCPDv3 and CLICpix sensors studied in this analysis. The red dotted line represents the CCPDv3 and the solid black line represents the CLICpix. From left to right; centred pixels, 1/4 offset (6.25 μm) and 1/2 offset (12.5 μm).

1.2 Construction

While replacing solder bump-bonding with a thin layer of glue in the construction of the sensors for the vertex detector offers benefits, such as reductions in the material budget and cost, the manufacturing procedure could lead to misalignments between the active pixel sensor and the readout ASIC. To determine the impact of these misalignments a number of sensors were constructed using the gluing procedure that contained offsets between the HV-CMOS and CLICpix, as shown in figure 1.3. A table 1.1 contains a summary of all the samples used in this study.

Assembly	Alignment
SET9	Centred
SET10	$\frac{1}{4}$ Offset
SET11	$\frac{1}{2}$ Offset
SET12	Centred
SET13	Centred
SET14	$\frac{1}{2}$ Offset
SET15	Centred
SET16	$\frac{1}{2}$ Offset

Table 1.1: Description of alignment of sensors.

The pitch of the pixels produced was 25 μm and the matrix size was 64×64. The full details of the gluing process can be found here (CERN NOTE CITE) along with a study into the absolute precision of the manufacturing procedure. It was found that for devices constructed in an identical fashion to those considered here, the glue layer

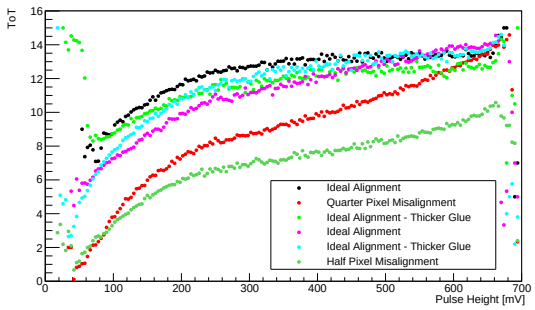

Figure 1.4: Average ToT vs pulse height.

thicknesses were less than 1 μm and the precision on the pixel positioning was less than 0.5 μm.

1.3 Device Characterisation

This section describes the electrical tests that were performed on the sensor designed to determine the properties of the HV-CMOS and CLICpix.

1.3.1 CLICPix Calibration

The first analysis was a radioactive source calibration. This test involved using a strontium 90

Compare the HV-CMOS pulse height to the ToT recorded on the CLICPix using strontium 90 sources. Gives indication of gluing layer and CLICPix capacitances.

- ToT vs pulse heights.
- ToT vs rise times.

1.3.2 Cross Couplings

ToT on adjacent cells vs pulse heights. No charge sharing apparent except for SET16. Possible issues with manufacturing other offset samples as some charge sharing is expcted.

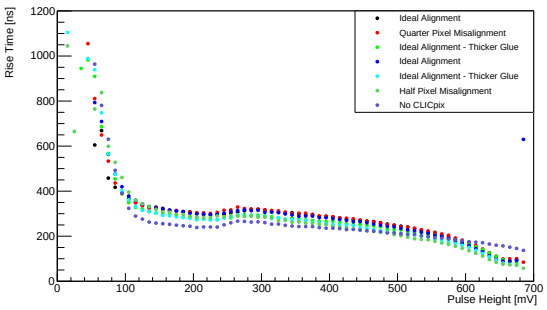

Figure 1.5: Rise time vs pulse height.

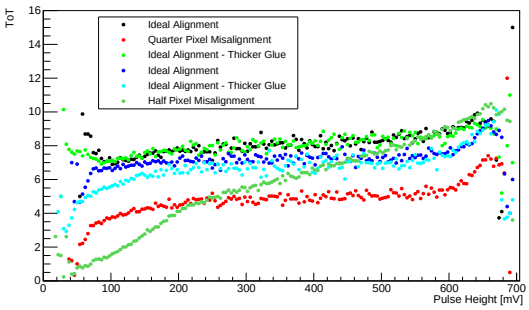

Figure 1.6: Average ToT on adjacent pixel vs pulse height.

1.3.3 Test Pulse Calibration

Inject pulse height of fixed size directly into CLICPix and recored ToT. This cannot be done for the HV-CMOS due to the device construction preventing getting to the relevant input to the HV-CMOS. Plots of average ToT vs pulse height, describe surrogate function fit and column structure.

1.4 Test Beam Analysis

1.4.1 Test Beam Area

Description of test beam, site and telescope.

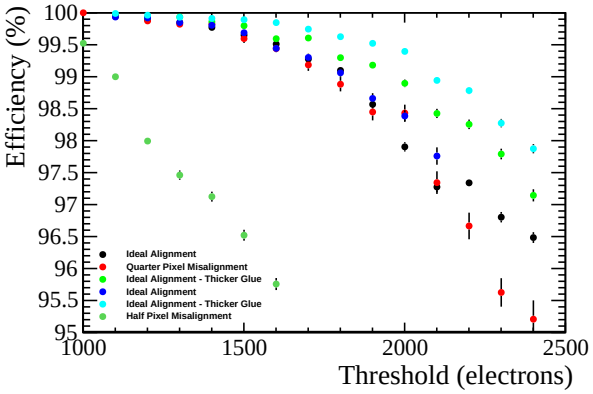

Figure 1.7: Efficiency vs threshold.

1.4.2 Efficiency

- Description of masks and why they need to be applied.
- Alignment description.
- Efficiency calculations and conclusions.

Chapter 2

The sensitivity of CLIC to anomalous gauge couplings through vector boson scattering

"Kids, you tried your best, and you failed miserably. The lesson is, never try."

— Homer Simpson

2.1 Motivation

Vector boson scattering is the interaction of the form VV $\rightarrow$ VV where V is any of the electroweak gauge bosons W^+, W^-, Z or γ. This is an interesting process to look at because it gives a detailed understanding of how the standard model Higgs is able to unitarise the otherwise unbounded cross section for longitudinal gauge boson scattering. Vector boson scattering also provides insights into beyond standard model physics that impacts the electroweak sector through the probing of anomalous triple and quartic gauge couplings. Presented in this section is an analysis into the sensitivity of CLIC to two of these anomalous quartic gauge couplings through the vector boson scattering process.

Triple and quartic gauge couplings lead to interactions of the form V $\rightarrow$ VV and VV $\rightarrow$ VV respectively. In the standard model there are five permissible vertices, shown in figure **??**, which arise from the kinematic term $\mathcal{L}_{kin} = -\frac{1}{4}B_{\mu\nu}B^{\mu\nu} - \frac{1}{4}W_{\mu\nu}W^{\mu\nu}$.

Anomalous triple and quartic gauge couplings are introduced as parameters in effective field theory models (EFTs). These anomalous couplings can either modify the standard model triple and quartic gauge boson couplings or introduce new triple and quartic couplings that were previously forbidden.

EFT models work under the assumption than new physics exists at an energy scale, Λ that is much higher than the energy scales currently accessible to modern day particle physics experiments. Furthermore, in limit $\Lambda \rightarrow \infty$ the standard model should be reproduced as the new physics becomes kinematically inaccessible. Such theories are also model independent, giving them a wide span in the search for new physics.

A classic example of an EFT theory is the Fermi theory for beta decay. The weak interaction occurring when a neutron decays into a proton, electron and anti-neutrino can be, at energies much below the mass of the W boson, can be treated as a four-point vertex with quartic coupling strength G_F, the Fermi Coupling constant. (Feynamn Diagram if keep)

This analysis examines the anomalous quartic gauge couplings α_4 and α_5, which are introduced as part of an EFT described in chapter THEORY CHAPTER. They appear in the Lagrangian through the following terms

$$\alpha_4[\mathrm{Tr}(V^\mu V_\mu)]^2 \text{ and } \alpha_5\mathrm{Tr}(V^\mu V_\nu)]\mathrm{Tr}(V^\nu V_\mu)] \tag{2.1}$$

where V_μ corresponds, in a carefully chosen gauge, to a linear combination of the massive gauge bosons W^+, W^- and Z. These terms affect the coupling constants for the standard model vertices $W^+W^- \rightarrow W^+W^-$ and $W^+W^- \rightarrow ZZ$ as well as introducing the new vertex $ZZ \rightarrow ZZ$. Vector boson scattering was an appropriate process to consider for a sensitivity study into the anomalous gauge couplings α_4 and α_5 as quartic gauge boson self-interaction vertices will be present in the dominant channels for such interactions (FEYNMAN DIAGRAM).

As CLIC is purposefully deigned for high precision measurements it is ideal for a study into vector boson scattering. The application of Particle Flow Calorimetry with

fine granularity calorimeters gives CLIC excellent jet energy resolution, which allows it to clearly characterise the multi-jet final states. When considering the invariant mass of these paired up jets, the nominal jet energy resolution for CLIC allows for accurate separation of W and Z bosons, which will be invaluable for event selection. This precision also helps CLIC to characterise final states containing missing energy in the form of neutrinos. The cross sections for the relevant processes are sufficiently large at the proposed running energies for CLIC to give a large sample size for this analysis. Finally, this study offers the potential to give results several orders of magnitude better than the complementary studies at the LHC due to the reduction in hadronic backgrounds and the high $\sqrt{s}$ for the interaction offered by colliding leptons instead of protons. All of the above reasons make a strong case for performing this analysis at CLIC.

This study focuses solely upon the vector boson scattering processes where the outgoing bosons decay purely hadronically. This decision was made as the hadronic channels are the dominant decay modes of the W and the Z boson, with branching fractions of the order of 70% for both (REFERENCE PDG), and given CLIC has excellent jet energy resolution . Therefore, the signal final states in this analysis are thus: $\nu\nu$qqqq, lνqqqq and llqqqq. Feynman diagrams involving vector boson scattering and containing these final states are shown in figure **??**.

2.2 Event Generation, Simulation and Reconstruction

Check this doesn't sound too close to Higgs paper.

Events were generated for this analysis using the Whizard [7, 11] 1.95 program. Due to the presence of beamstrahlung photons in the CLIC beam events were generated from collisions of e^+e^-, $e^+\gamma$, γe^- and $\gamma\gamma$. The energy spectra used for all particles involved in these collisions accounted for the effects of radiation in the form of beamstrahlung photons and the intrinsic energy spread of the CLIC beam. Furthermore, events involving the interaction between the electromagnetic field of the beam particles involving quasi-real photon mediators with low momenta, described by the Weizsacker-Williams approximation or the Equivalent Photon Approximation (EPA), were generated using Whizard and included in this analysis. Fragmentation and hadronisation was implemented using PYTHIA 6.4 [12], which was tuned for OPAL e^+e^- collision data recorded at LEP (see [8] for details). The decays of tau

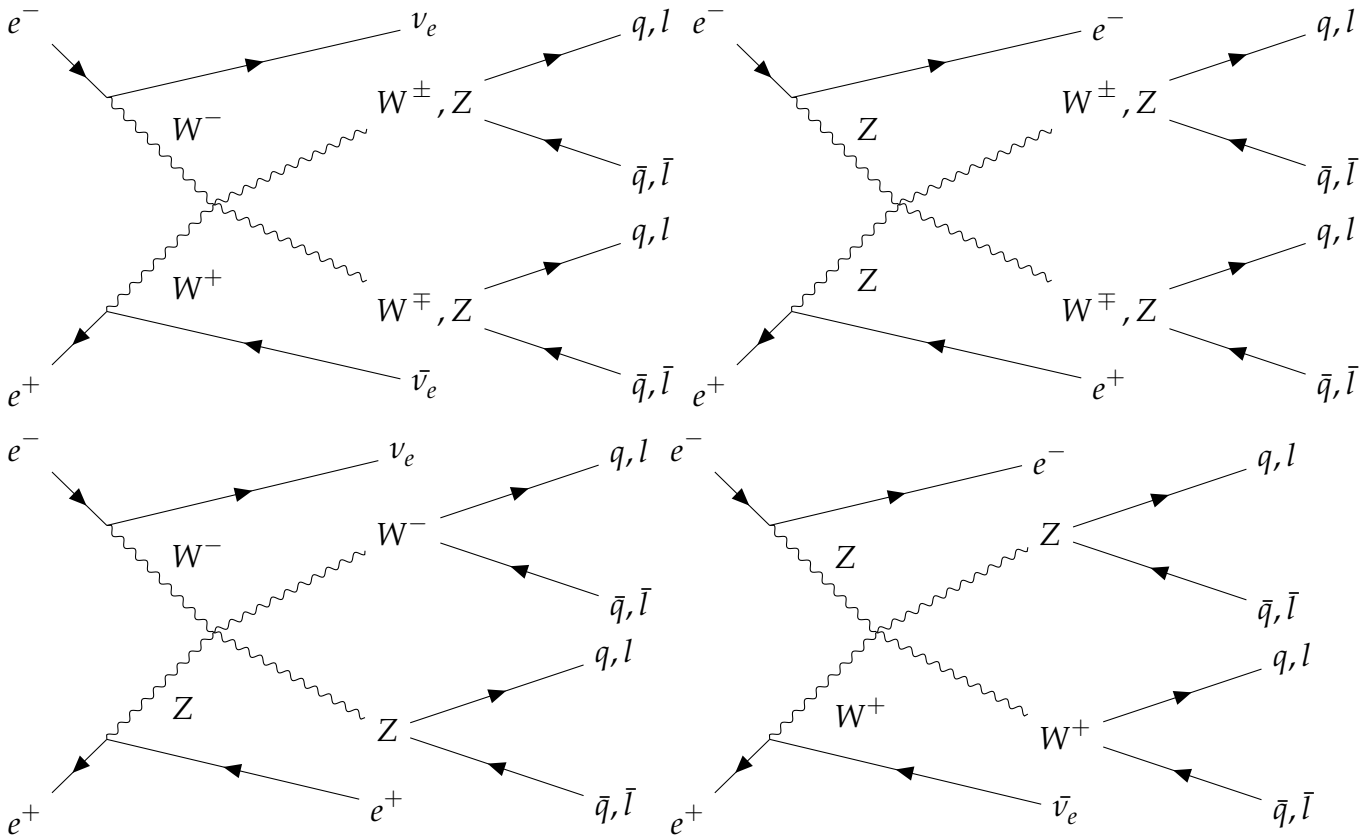

Figure 2.1: Feynman diagram of vector boson scattering at CLIC. q = u, d, s, b, c and l = e, μ, τ, ν_e, ν_ν, ν_τ

leptons was simulated using Tauola [14]. The full list of events simulated for this analysis, along with their standard model cross section at 1.4 TeV can be found in table 2.1. The samples generated comprise all final states that would be relevant either as signal or background processes, for an analysis involving the purely hadronic decay channels involved in a vector boson scattering process. In full they are:

- Vector boson scattering signal final states that are expected to show sensitivity to the anomalous couplings: $e^+e^- \to \nu\nu qqqq$, $e^+e^- \to l\nu qqqq$ and $e^+e^- \to llqqqq$
- Four jet final states arising from e^+e^- interactions: $e^+e^- \to qqqq$.
- Two jet final states arising from e^+e^- interactions: $e^+e^- \to \nu\nu qq$, $e^+e^- \to l\nu qq$, $e^+e^- \to llqq$ and $e^+e^- \to qq$.
- Four jet final states arising from the interactions of either e^+ or e^- with a beamstrahlung photon: $\gamma_{BS}e^- \to qqqqe^-$, $e^+\gamma_{BS} \to qqqqe^+$, $\gamma_{BS}e^- \to qqqq\nu$ and $e^+\gamma_{BS} \to qqqq\nu$.
- Four jet final states arising from the interactions of either e^+ or e^- with the electromagnetic field of the opposing beam particle. These cross sections are calculated using the EPA approximation, which represents the electromagnetic field of the opposing beam particle as a series of photons and so the final states appear as interactions of e^+ or e^- with photons: $\gamma_{EPA}e^- \to qqqqe^-$, $e^+\gamma_{EPA} \to qqqqe^+$, $\gamma_{EPA}e^- \to qqqq\nu$ and $e^+\gamma_{EPA} \to qqqq\nu$.
- Four jet final states arising from the interaction of the electromagnetic fields of opposing beam particles using the EPA approximation: $\gamma_{EPA}\gamma_{EPA} \to qqqq$.
- Four jet final states arising from the interaction of the electromagnetic field of either e^+ or e^- using the EPA approximation with a beamstrahlung photon: $\gamma_{EPA}\gamma_{BS} \to qqqq$ or $\gamma_{BS}\gamma_{EPA} \to qqqq$.
- Four jet final states arising from the interaction of two beamstrahlung photons: $\gamma_{BS}\gamma_{BS} \to qqqq$.

Note: In the above list q = u, d, s, c and b, l = e, μ, τ and $\nu = \nu_e$, ν_μ and ν_τ.

The samples used in this analysis were simulated with the CLID_ILD detector model [1]. The simulation was performed in MOKKA [10], a GEANT4 [2] wrapper providing detailed geometric descriptions of detector concepts for the linear collider. Events were reconstructed using MARLIN [5], a c++ framework designed for recon-

struction at the linear collider. PandoraPFA [9, 13] was used to apply Particle Flow Calorimetry in the reconstruction, the full details of which can be found in chapter PANDORA CHAPTER.

The CLIC_ILD is a variant of the ILD detector described in section REFERENCE. The only significant difference between the modles is that CLIC_ILD has a 60 layer scintillator-tugsten HCal in comparison to the 48 layers found in the default ILD detector. The thicknesses of the layers in the HCal models are identical, so the extra layers correspond to an increase in the total thickness of the HCal. This is needed to compensate for the effects of leakage at the higher energies seen by the CLIC experiment in comparison to the ILC.

2.3 Modelling of Anomalous Gauge Couplings

It was necessary when generating samples that are sensitive to the anomalous gauge couplings α_4 and α_5 to use Whizard version 1.97, instead of the previously quoted version 1.95. This change was required as version 1.97 contained a unitarisation scheme that ensured cross sections for processes involving longitudinal gauge boson scattering were bound the energies considered i.e. the TeV scale.

The sensitivity of an individual event to the anomalous gauge couplings is determined through an event weight. This weight is given by the ratio of the squares of the matrix element used in the cross section calculation, one matrix element using non-zero values of α_4 and α_5 and the other matrix element using the standard model values of α_4 and α_5, i.e. 0. The weight varies as a function of α_4 and α_5 as well as varying on an event by event basis as the kinematics of the final state changes. Examples of the event weights as a function of α_4 and α_5 for selected events is shown in figure 2.2 for 1.4 TeV $\nu\nu$qqqq final state events.

This reweighting procedure has many advantages over the alternative of generating new samples with fixed α_4 and α_5, notably the absence of systematic errors arising from new event generation, simulation and reconstruction. Only final states showing a sensitivity to α_4 and α_5 require reweighting and to determine those states a comparison was made between the cross section using the standard model values of α_4 and α_5, i.e. 0, and the same calculation using non-zero values of these couplings at 1.4 TeV. This

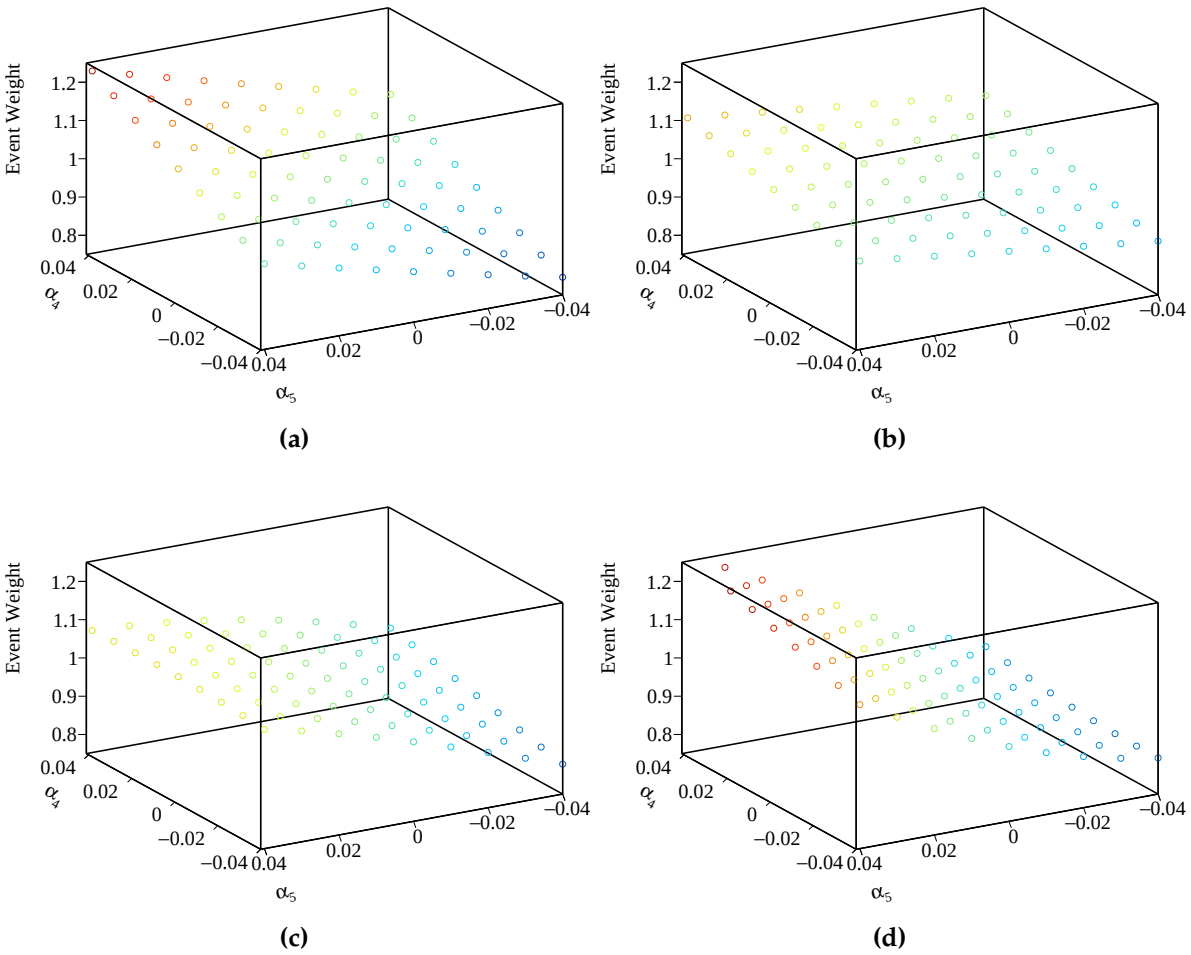

Figure 2.2: A selection of plots showing how the event weight changes when varying the anomalous couplings α_4 and α_5 for 1.4TeV $\nu\nu$qqqq final state events.

Final State	Cross Section 1.4 TeV [fb]
$e^+e^- \to \nu\nu qqqq$	24.7
$e^+e^- \to l\nu qqqq$	110.4
$e^+e^- \to llqqqq$	62.1
$e^+e^- \to qqqq$	1245.1
$e^+e^- \to \nu\nu qq$	787.7
$e^+e^- \to l\nu qq$	4309.7
$e^+e^- \to llqq$	2725.8
$e^+e^- \to qq$	4009.5
$\gamma_{EPA}e^- \to qqqqe^-$	287.1
$\gamma_{BS}e^- \to qqqqe^-$	1160.7
$e^+\gamma_{EPA} \to qqqqe^+$	286.9
$e^+\gamma_{BS} \to qqqqe^+$	1156.3
$\gamma_{EPA}e^- \to qqqq\nu$	32.6
$\gamma_{BS}e^- \to qqqq\nu$	136.9
$e^+\gamma_{EPA} \to qqqq\nu$	32.6
$e^+\gamma_{BS} \to qqqq\nu$	136.4
$\gamma_{EPA}\gamma_{EPA} \to qqqq$	753.0
$\gamma_{EPA}\gamma_{BS} \to qqqq$	4034.8
$\gamma_{BS}\gamma_{EPA} \to qqqq$	4018.7
$\gamma_{BS}\gamma_{BS} \to qqqq$	21406.2

Table 2.1: Cross sections of signal and background processes at 1.4 TeV. In the above table $q \in u, \bar{u}, d, \bar{d}, s, \bar{s}, c, \bar{c}, b$ or $\bar{b}$ while $l \in e^\pm, \mu^\pm$ or $\tau^\pm$ and $\nu \in \nu_e, \nu_\mu$ and ν_τ. The subscript EPA or BS for the incoming photons indicate whether the photon is generated from the equivalent photon approximation or beamstrahlung.

comparison was performed on all of the generated samples listed in table 2.1 and the results for samples showing sensitivity to the couplings can be found in table 2.2

The cross sections were found to differ when using non-zero values for the anomalous couplings in comparison to the standard model prediction only for the vector boson scattering signal final states $\nu\nu qqqq$, $l\nu qqqq$ and $llqqqq$. In reality, non-zero anomalous couplings would change the cross sections of all processes considered, however, the sensitivity would only arise from high order terms in the Lagrangian. Such terms would not be dominant in determining the cross section and so are omitted

from the generator making certain final states appear invariant to changes in the anomalous couplings.

Final State	Cross Section [fb] ($\alpha_4 = \alpha_5 = 0.00$)	Cross Section [fb] ($\alpha_4 = \alpha_5 = 0.05$)	Percentage Change[%]	CLIC Cross Section [fb]
$e^+e^- \to \nu\nu qqqq$	20.8	34.6	+66.3	24.7
$e^+e^- \to l\nu qqqq$	112	113	+0.9	115.3
$e^+e^- \to llqqqq$	59.7	68.6	+14.9	62.1

Table 2.2: Cross section for selected processes for given value of α_4 and α_5 at 1.4 TeV.

The cross section calculations show that the most sensitive final state to the anomalous gauge couplings is $\nu\nu$qqqq, therefore, this analysis will focus entirely upon this final state. Furthermore, as the lνqqqq final state has a much reduced sensitivity in comparison to the $\nu\nu$qqqq state and as the llqqqq can be easily vetoed from the analysis, as will be shown in subsequent chapters, it is only necessary to consider the sensitivity of the $\nu\nu$qqqq final state. For the aforementioned reasons the lνqqqq and llqqqq final states will be treated as backgrounds that are invariant to changes in the anomalous couplings α_4 and α_5.

In order to determine the anomalous gauge coupling sensitive event weights it was necessary to use the anomalous gauge coupling model in Whizard, which enforces a unit CKM matrix. In the context of vector boson scattering and the $\nu\nu$qqqq final state, which is the only final state requiring reweighting, this restricts the decays of the W^- boson to d$\bar{u}$ and s$\bar{c}$, the W^+ boson to u$\bar{d}$ and c$\bar{s}$ and the Z boson to u$\bar{u}$, d$\bar{d}$, s$\bar{s}$, c$\bar{c}$ and b$\bar{b}$. In comparison, the non-unit CKM matrix allows for extra decay modes, however, this was found to have a negligible effect on the samples when comparing several reconstructed level distributions. Furthermore, flavour tagging of jets was not used in this analysis as it offered negligible gains when performing event selection and so any bias in quark flavour present due to the enforcement of a unit CKM in the signal samples did not impact this analysis.

2.4 Data Analysis

The focus of this section is to describe the post reconstruction procedure applied to the signal and background events, described in **??**, to extract the relevant information needed for this sensitivity study.

2.4.1 Jet Finding

After the reconstruction two further processors are applied to remove reconstructed particle flow objects (PFOs) that originate from beam related backgrounds, described in section CLIC BEAM CHAPER, from the event. The first processor is the CLICTrack-Selection, designed to veto poorly reconstructed tracks and to reject tracks where the time of arrival at the calorimeter between the helix fit to the track and to a straight line of flight differ by 50ns. The latter would indicate the tracked particle does not create the calorimetric energy deposits that it has been associated to. The second processor is the CLICPfoSelector, which applies cuts to the p_{T} and timing information of the PFOs. These cuts vary as a function of position in the detector and the reconstructed particle type in an attempt to target the regions of the detector where background, primarily low p_{T} $\gamma\gamma \rightarrow$ Hadrons events, are more prominent. Three configurations of the CLICPfoSelector have been developed for the CLIC environment and were considered for this analysis. They are, in order of increasing background rejection, the Loose, Default and Tight selections. Tthe full details of each can be found here [9].

After the application of the CLICTrackSelection and CLICPfoSelector the MarlinFastJet processor, a wrapper for the FastJet [4] processor, was used to cluster the events into four jets. These jets are then paired up to form two candidate bosons. This pairing is performed on the assumption that the correct pairing is achieved when the difference between the invariant masses of the jet pairs is a minimum. In the case of the signal final state, $\nu\nu$qqqq, it is assumed that the four jets have arisen from the hadronic decays of the outgoing bosons involved in the vector scattering process and that the pairing of the jets gives candidate bosons that match the outgoing bosons involved in vector boson scattering.

The jet clustering was done using the longitudinally invariant k_t jet algorithm in exclusive mode. In contrast to the inclusive mode, the exclusive mode allows the user

to request a fixed number of jets in the output from MarlinFastJet. The longitudinally invariant k_t algorithm proceeds as follows:

- For each pair of particles, i and j, the k_t distance, d_{ij}, and beam distance, $d_{iB} = p_t^2$, are calculated.

$$d_{ij} = \min(p_{ti}^2, p_{tj}^2)\Delta R_{ij}^2 / R^2 \tag{2.2}$$

  where $\Delta R_{ij}^2 = (y_i - y_j)^2 + (\phi_i - \phi_j)^2$, p_t is the transverse momentum of the particle with respect to the beam axis, y_i is the rapidity of particle i and ϕ_i is the azimuthal angle of particle i. R is a configurable parameter that typically is of the order of 1.

- The minimum distance, d_{min}, of all the k_t and beam distances is found. If the minimum occurs for a k_t distance, merge particles i and j, summing their 4-momenta in the energy combination scheme. If the beam distance is the minimum, declare particle i to be apart of the "beam" jet. Remove this particle from the list of particles and do not included in the final jet output.

- Repeat until the requested number of jets have been created, or inclusive mode no particles are left in the event.

Two other clustering algorithms were considered, but, as figure 2.3 shows, were found to be inappropriate for the experimental conditions at CLIC. These alternative algorithm choices are applied in the same manor as the longitudinally invariant k_t algorithm, however, they differ in their for the k_t distance, d_{ij}, and beam distance, d_{iB}.

The first alternative jet algorithm considered was the k_t algorithm for e^+e^- colliders (or Durham algorithm) where $d_{ij} = 2\min(E_i^2, E_j^2)(1 - cos\theta_{ij})$ and d_{iB} is not used. θ_{ij} is the opening angle of particles i and j meaning that in the collinear limit d_{ij} corresponds to the relative transverse momenta of the particles. The major failure of this algorithm when applied to CLIC is the absence of d_{iB}, which leads to many beam related background particles being associated to jets. As figure 2.3 shows, the invariant mass of the paired jets, which is expected to be centred around the W and Z boson masses, is much larger than expected, due to the presence of the beam related backgrounds in the jets. Also this algorithm is not invariant to boosts along the beam direction making it inappropriate to use at CLIC as the beam induced backgrounds modify the nominal collision kinematics.

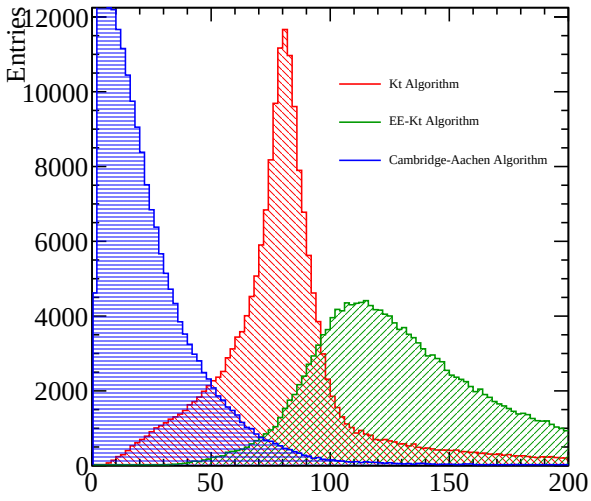

(a)

Figure 2.3: Reconstructed masses for different choices of jet algorithm for 1.4 TeV $\nu\nu$qqqq events. These masses arise by forcing the reconstructed events into 4 jets and then pairing up the jets into pairs such that the reconstructed invariant masses of the pairs are closest to each other. These samples should be dominated by vector boson scattering involving pairs of W bosons and so it is expected that a peak at the W boson true mass should be observed. As this does not occur for the Cambridge-Aachen algorithm or the ee_kt algorithm they were deemed unsuitable for this analysis at both 1.4. In the case of the kt algorithm and the ee_kt algorithm an R parameter of 0.7 was used.

The second alternative jet algorithm considered was the Cambridge/Aachen jet algorithm where $d_{ij} = \Delta R_{ij}^2 / R^2$ and $d_{iB} = 1$. This algorithm gave poor performance as does not account for the transverse momentum or energy of the particles being clustered. In essence, this is a cone clustering algorithm with a cone radius defined through $\Delta R_{ij} = R$, which even for large R was found to discard too much energy in the event to be useful for this analysis. This can be seen in figure 2.3 as the invariant mass of the paired jets is much lower than expected. This algorithm is useful for events with highly boosted jets, but at CLIC the jets are too disperse for this algorithm to be successfully applied.

Optimal Jet Finding Algorithm

Optimisation of the jet algorithm configuration was performed on the choice of PFO selection as well as the value of the R parameter used in the longitudinally invariant

k_t algorithm. The optimal configuration for the jet algorithm at 1.4 TeV was found to use default selected PFOs and an R parameter of 0.9.

The procedure involved performing the sensitivity study, described in section BLAH**??**, using solely the $\nu\nu$qqqq signal final state. This procedure leads to the construction of a χ^2 surface from which confidence contours can be extracted in the α_4 and α_5 space. The χ^2 surface for the optimal jet configuration at 1.4 TeV using the $\nu\nu$qqqq signal final state is shown in figure 2.4a. This procedure ensured that the optimisation was done with respect to the physics of interest without having to perform the jet reconstruction procedure for the large number of background events.

Confidence limits on the individual parameters α_4 and α_5 were determined by setting the corresponding coupling term to zero and examining the now one dimensional χ^2 distribution. A fourth order polynomial was fitted to the minima of this distribution and the one sigma confidence limit defined using $\Delta\chi^2$ of 1. $\Delta\chi^2$ is defined as the change in χ^2 with respect to the minima in the χ^2 surface. Note that for the two dimensional χ^2 surface a one sigma confidence limit is given by a $\Delta\chi^2$ of 2.28 due to the additional degree of freedom in the fit. The one dimensional χ^2 distribution for α_4 and α_5, assuming $\alpha_5 = 0$ and $\alpha_4 = 0$ respectively, for the optimal jet configuration at 1.4 TeV using the $\nu\nu$qqqq signal final state is shown in figures 2.4b and 2.4c. Using these distributions the one sigma confidence limits on α_4 is -0.0038 to 0.0047 and on α_5 is -0.0027 to 0.0030.

2.4.2 Lepton Finding

An isolated lepton finder was included in the analysis chain in an attempt to reject background events containing leptons. The isolated lepton finder attempts to find whether a PFO is an electron or muon based on the calorimetric energy deposits before then placing cuts on the tracks associated to the PFOs to determine whether the tracks originate from the impact point. Finally isolation cuts restricting the energy in a cone surrounding the PFO are applied to ensure the particles does not belong to a jet. The efficiency of the lepton finder is summarised in table 2.3.

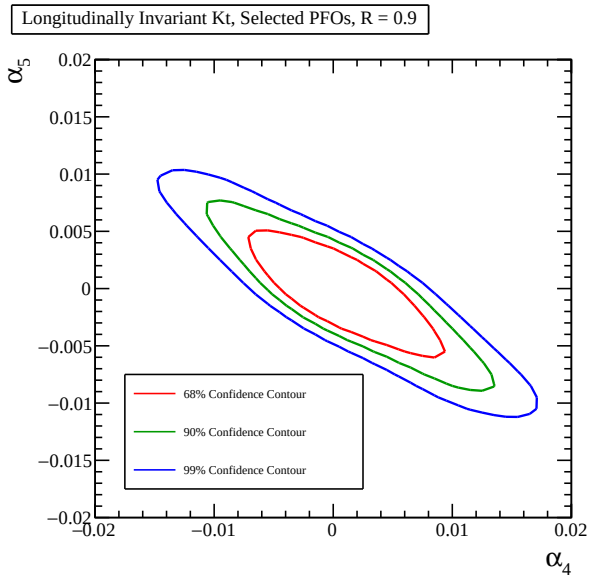

(a) χ^2 sensitivity contours in α_4 and α_5 space.

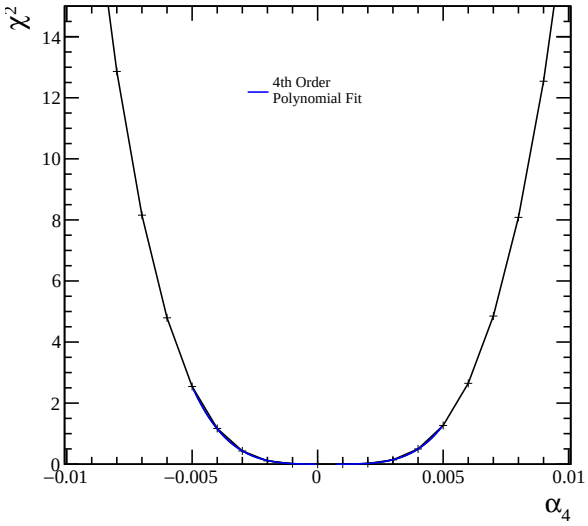

(b) χ^2 as a function of α_4 assuming $\alpha_5 = 0$.

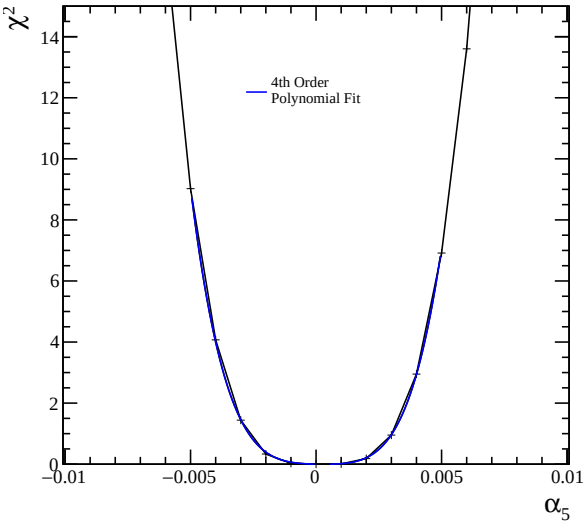

(c) χ^2 as a function of α_5 assuming $\alpha_4 = 0$.

Figure 2.4: χ^2 sensitivity distributions for the qqqq$\nu\nu$ final state arising from a fit to $\cos\theta^*_{\text{Jets}}$ at 1.4 TeV for the optimal jet reconstruction parameters.

Final State	$\epsilon_{\text{Lepton Finding}}$
$e^+e^- \to \nu\nu qqqq$	99.7
$e^+e^- \to l\nu qqqq$	48.9

Table 2.3: The efficiency of isolated lepton finding at 1.4 TeV for the $\nu\nu$qqqq and lνqqqq final states. Efficiency here is defined as the fraction of events where no isolated leptons were found.

2.4.3 Discriminant Variables

The next stage of the analysis involved the calculation of a number of event-based variables that were found to be useful for this analysis. The variables that were calculated are as follows:

- **Particle level** variables:
  - Number of PFOs.
  - Particle type and energy of the highest energy PFO.
  - Energy of the highest energy electron.
  - Cosine of the polar angle of the highest energy track.
- **Candidate boson** variables:
  - Energy of candidate bosons.
  - Invariant mass of the bosons.
  - Acolinearity of the boson pair, which is defined as 180 degrees minus the opening angle of the pair of bosons in the rest frame of the detector.
  - Acolinearities of the jets forming each of the candidate bosons.
  - Cos(θ^*_{Bosons}). Cosine of the opening of the bosons in the rest frame of the boson pair.
  - Cos(θ^*_{Jets}). Cosine of the opening of the jets forming each candidate in the rest frame of the candidate boson.
- **Event based** variables:
  - The invariant mass of the visible system.

- The vector sum of the transverse momentum of all PFOs in the event.
- The cosine of the polar angle of the missing 3-momentum assuming a collision at the nominal centre of mass energy.
- Principle thrust T, defined through the following equation

$$T = \max_{\bar{\mathbf{n}}}\left(\frac{\Sigma_i \mathbf{p}_i.\bar{\mathbf{n}}}{\Sigma_i |\mathbf{p}_i|^2}\right) \tag{2.3}$$

  Where p_i are the components of the momenta of PFO i in the rest frame of the detector, $\bar{\mathbf{n}}$ is unit vector and the sum Σ_i runs over all particles in the event.
- Sphericity, defined through the sphericity tensor S^{ab}:

$$S^{ab} = \frac{\Sigma_i p_i^\alpha p_j^\alpha}{\Sigma_{i,\alpha=1,2,3} |p_{i|}^\alpha|^2} \tag{2.4}$$

  Where p_i are the components of the momenta of PFO i in the rest frame of the detector and the sum Σ_i runs over all particles in the event. Sphericity is defined as $\mathrm{S} = \frac{3}{2}(\lambda_2 + \lambda_3)$, where λ_i are the eigenvalues of the sphericity tensor defined such $\lambda_1 \geq \lambda_2 \geq \lambda_3$. This provides a measure of how spherical the reconstructed event topology is with isotropic events having $S \approx 1$, while two jet events have $S \approx 0$.
- Aplanarity defined as $\frac{3}{2}\lambda_3$ where λ_3 is an eigenvalue of the sphericity tensor. This provides a measure of whether an event is linear or planar in shape.

- **Jet clustering parameter** variables, y_{ij} where $i = 1, 2, 3, 4, 5, 6$ and $j = i + 1$. These are the smallest k_t distance found when combining j jets into i jets. Note: -log10 yij cut on.

2.5 Event Selection

As described in section 2.3 the signal final state in this analysis is the $\nu\nu$qqqq final state, while the backgrounds consist of all 2 and 4 jet final stats that could be confused for the signal state in the reconstruction. A complete list of signal and background final states used for this analysis, alongside their standard model cross sections, can be found in table 2.1. In an attempt to isolate signal from background an event selection procedure

consisting of a set of preselection cuts followed by the application of a multivariate analysis (MVA) was applied to this data set and the full details of those are given in the following section.

2.5.1 Pre Selection

A refined selection of the $\nu\nu$qqqq signal final state is achieved using MVA. However, to ensure efficiency in the training and application of that MVA a number of simple preselection cuts were developed that veto obvious background final states prior to the application of the MVA. These cuts were developed such that as much background as possible would be rejected, while retaining enough signal to make the analysis viable. Preselection cuts were applied to the transverse momentum, invariant mass of the visible system and the number of isolated leptons. The raw distributions of these variables is.shown in figure **??** and based on these distributions the following cuts were applied:

- Transverse momentum > 100 GeV. This cut is effective due to the presence of missing energy in the form of neutrinos in the signal final state.
- Visible mass of the system > 200 GeV. This cut was effective against the $\nu\nu$qq and νlqq final states. These states would be dominated by the channels involving a single W or Z boson propagator decaying hadronically, as shown in figure **??** and therefore the invariant mass of the visible system peaks around the W and Z mass. This is not the case for the $\nu\nu$qqqq signal final state, which typically has a much larger visible mass.
- Number of isolated leptons = 0. This cut vetoes events with leptons in the final state.

The impact of these preselection cuts can be found in table FINAL SUMMARY TABLE REF **??**.

2.5.2 MVA

Having established the preselection cuts a MVA was applied, using the TMVA toolkit [6], to refine the event selection. The signal and background final state samples were halved; one half sample was used to train the MVA and the remaining half sample was

used in the subsequent analysis. The halving of the signal and background sample had minimal impact on the analysis as all event numbers were normalised to the correct luminosity for CLIC running at 1.4 TeV and the sample size was sufficiently large.

The following variables were used for training of the MVA:

- Number of PFOs in the event.
- Particle type and energy of the highest energy PFO in the event.
- Energy of the highest energy electron in the event.
- Cosine of the polar angle of the highest energy track in the event.
- Energy and invariant mass of the candidate bosons.
- Acolinearity of the boson pair.
- Acolinearities of the jets forming each of the candidate bosons.
- The vector sum of the transverse momentum of all PFOs in the event.
- The cosine of the polar angle of the missing 3-momentum assuming a collision at the nominal centre of mass energy.
- Principle thrust.
- Sphericity and aplanarity.
- The jet clustering parameter y_{ij} where $i = 1, 2, 3, 4, 5, 6$ and $j = i + 1$.

A variety of MVA options were considered and it was found that the optimal algorithm was the boosted decision tree (BDT) as shown by figure **??**.

The BDT was further optimised by varying the number of trees used, the depth of the trees and the number of cuts applied and an optimal significance, $S/\sqrt{(S + B)}$, of 53.6 was obtained.

2.5.3 Event Selection Summary

The event selection is summarised using the distribution of the invariant mass of the candidate bosons, which for the signal final state should peak around the W and Z masses. This distribution is shown in figure 2.6 with no event selection, with

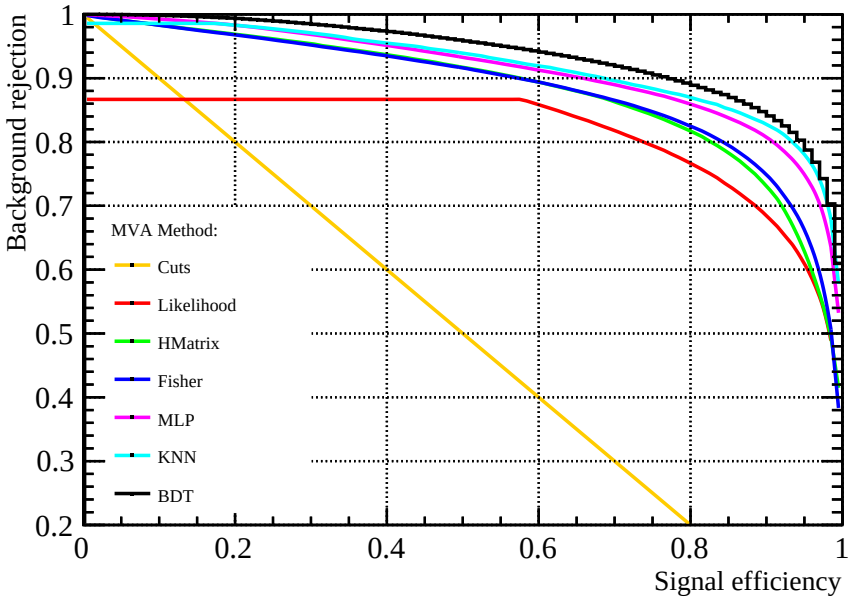

Figure 2.5: Background rejection as a function of signal efficiency for a variety of MVA options at 1.4 TeV.

the preselection cuts and with both preselections cuts and MVA applied. The event selection is also summarised using the efficiencies that are shown in table 2.4.

As expected the dominant background processes after the MVA is applied are those that will look identical to the visible signal process i.e. qqqq and missing energy. Two smaller sources of background that pass the MVA exists, those where two jets and missing energy are confused as four jets and missing energy and those where a lepton is not properly reconstructed and the events look like four jets and missing energy.

2.6 Effect of Anomalous Coupling/Fitting Methodology

This sections describes the procedure used for constructing the χ^2 surface and the subsequent confidence contours used to determine the sensitivity of CLIC to the anomalous gauge couplings α_4 and α_5.

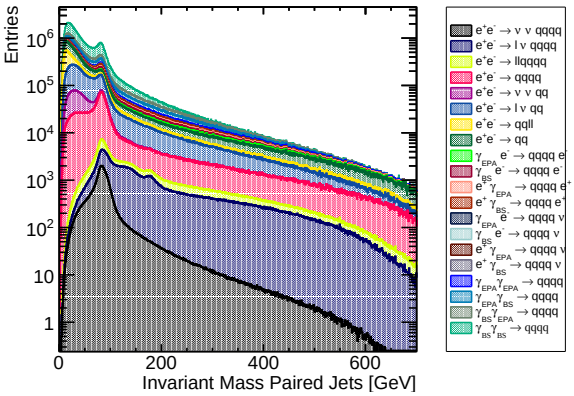

(a) No cuts applied.

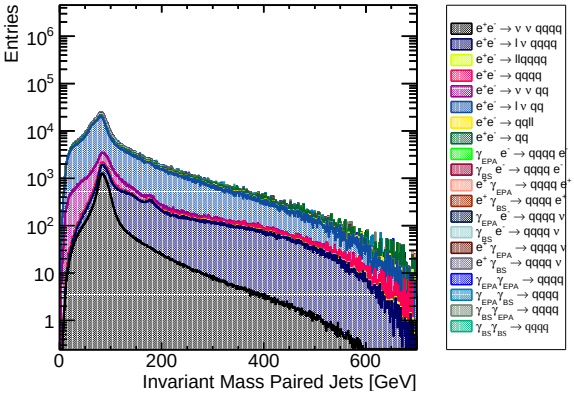

(b) Preselection cuts applied.

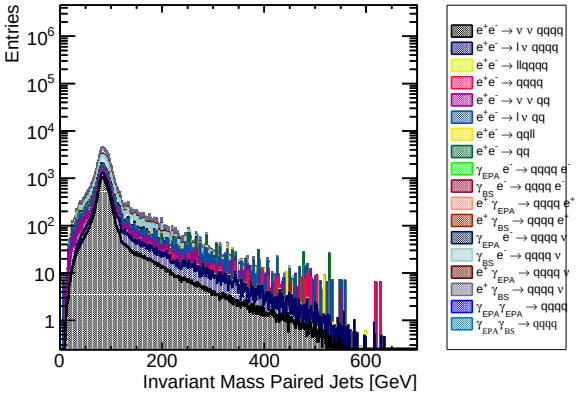

(c) Preselection cuts and MVA applied.

Figure 2.6: Impact of preselection and MVA on the reconstructed invariant mass of the bosons arising from jet pairing at 1.4 TeV.

Final State	ϵ_{presel}	ϵ_{BDT}	N_{BDT}
$e^+e^- \to \nu\nu qqqq$	56.7%	39.9%	14,770
$e^+e^- \to l\nu qqqq$	25.7%	3.7%	6,159
$e^+e^- \to llqqqq$	0.7%	0.1%	80
$e^+e^- \to qqqq$	8.8%	0.1%	1,264
$e^+e^- \to \nu\nu qq$	4.3%	0.3%	3,286
$e^+e^- \to l\nu qq$	8.8%	0.1%	6,262
$e^+e^- \to llqq$	0.1%	-	234
$e^+e^- \to qq$	0.6%	-	1,016
$\gamma_{\text{EPA}}e^- \to qqqqe^-$	0.2%	-	20
$\gamma_{\text{BS}}e^- \to qqqqe^-$	0.1%	-	42
$e^+\gamma_{\text{EPA}} \to qqqqe^+$	0.3%	-	19
$e^+\gamma_{\text{BS}} \to qqqqe^+$	-	-	44
$\gamma_{\text{EPA}}e^- \to qqqq\nu$	18.0%	7.3%	3,552
$\gamma_{\text{BS}}e^- \to qqqq\nu$	23.2%	12.0%	18,540
$e^+\gamma_{\text{EPA}} \to qqqq\nu$	18.2%	7.5%	3,652
$e^+\gamma_{\text{BS}} \to qqqq\nu$	23.4%	12.2%	18,770
$\gamma_{\text{EPA}}\gamma_{\text{EPA}} \to qqqq$	0.2%	-	68
$\gamma_{\text{EPA}}\gamma_{\text{BS}} \to qqqq$	0.1%	-	55
$\gamma_{\text{BS}}\gamma_{\text{EPA}} \to qqqq$	-	-	0
$\gamma_{\text{BS}}\gamma_{\text{BS}} \to qqqq$	-	-	0

Table 2.4: Selection summary at 1.4TeV. The subscript EPA or BS for the incoming photons indicate whether the photon is generated from the equivalent photon approximation or beamstrahlung. Cells omitting the efficiency indicate an efficiency of less than 0.1%.

2.6.1 Sensitive Distribution

The sensitivity of CLIC to the anomalous gauge couplings is determined through the use of a χ^2 fit to the distribution of $\cos\theta^*_{Jets}$. For a given event, the jet clustering and pairing proceeds as described in section **??** and leads to the event being clustered into four jets, which are then paired up to give two candidate bosons. θ^*_{Jets} is defined as the opening angle of the jets in the rest frame of these candidate bosons. The distribution of $\cos\theta^*_{Jets}$ proved to be highly sensitive to the anomalous gauge couplings as shown in figure 2.7.

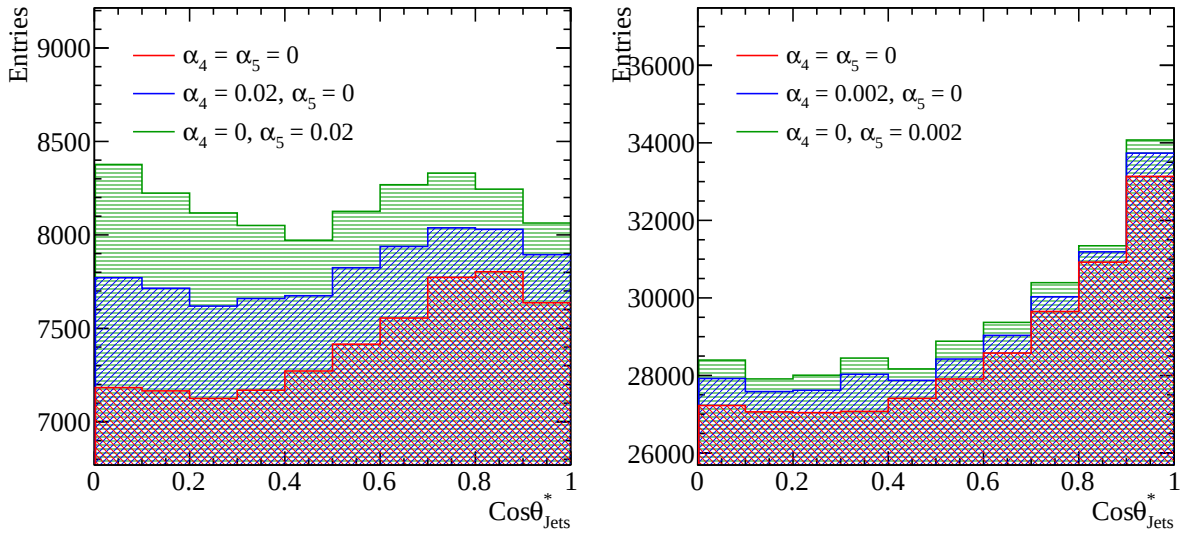

(a) 1.4 TeV Events

(b) 3 TeV Events

Figure 2.7: Sensitivity of $\cos\theta^*_{Jets}$ to anomalous couplings at 1.4 and 3 TeV. The jet algorithm used for this example was the longitudinally invariant kt algorithm with an R parameter of 0.7. This sample corresponds to pure signal of hadronic decays in vector boson scattering i.e. $\nu\nu$qqqq.

The distribution of $\cos\theta^*_{Bosons}$ was also considered for this sensitivity study, however, it proved to be less sensitive than $\cos\theta^*_{Jets}$. This can be seen when comparing figures 2.7 and 2.8. θ^*_{Bosons} is defined as the opening angle between the two candidate bosons two bosons in the rest frame of the candidate boson pair. Furthermore, it was found that the χ^2 distribution formed from the two dimensional distribution of $\cos\theta^*_{Jets}$ against $\cos\theta^*_{Bosons}$ did not significantly benefit the sensitivity in comparison using the one dimensional distribution of $\cos\theta^*_{Jets}$ and therefore was not considered for this analysis.

2.6.2 χ^2 Surface Definition

The χ^2 surface is defined through the following equation:

$$\chi^2 = \Sigma_i \frac{(O_i - E_i)^2}{E_i} \tag{2.5}$$

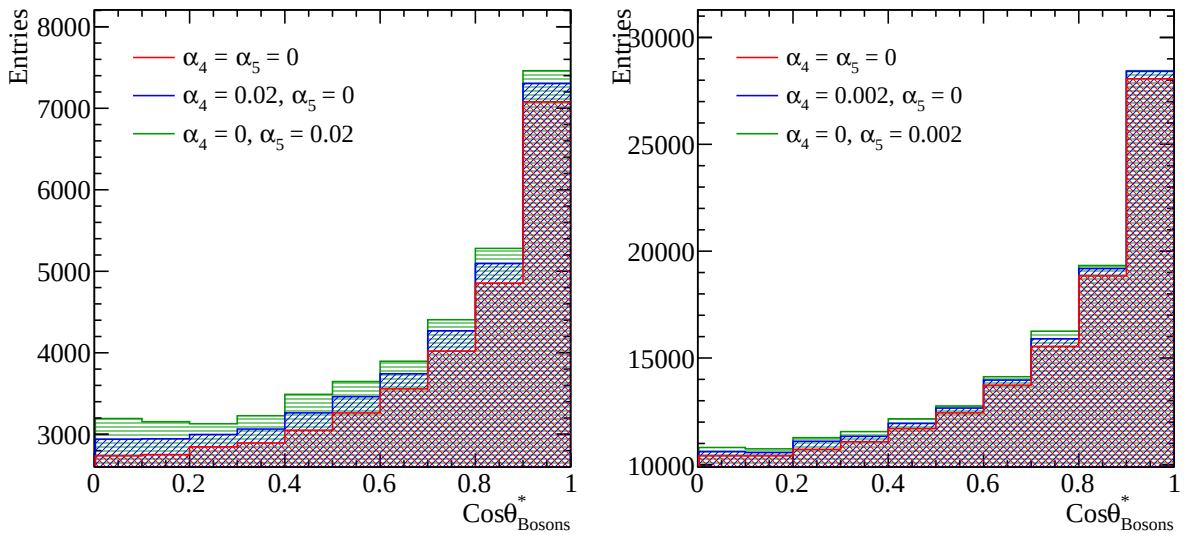

(a) 1.4 TeV Events **(b)** 3 TeV Events

Figure 2.8: Sensitivity of $\cos\theta^*_{Bosons}$ to anomalous couplings at 1.4 and 3 TeV. The jet algorithm used for this example was the longitudinally invariant kt algorithm with an R parameter of 0.7. This sample corresponds to pure signal of hadronic decays in vector boson scattering i.e. $\nu\nu$qqqq.

Where O_i is the observed, $\alpha_4 = \alpha_5 = 0$, bin content for bin i in the distribution of $\cos\theta^*_{Jets}$, E_i is the expected, $\alpha_4 \neq 0$ and $\alpha_5 \neq 0$, bin content for bin i in the distribution of $\cos\theta^*_{Jets}$ and Σ_i is the sum over the bins of the $\cos\theta^*_{Jets}$ distribution. The distribution of $\cos\theta^*_{Jets}$ was binned in a histograms containing 10 bins ranging from 0 to 1, as shown in figure 2.7. This binning was selected to maximise the sensitivity of the distribution, while minimising the effect of large bin by bin fluctuations arising from individual events with large event weights.

Confidence limits that describe the sensitivity of CLIC to the anomalous gauge couplings, were found by examining the χ^2 surface in α_4 and α_5 space. Deviations about the minima of this surface, which by construction occurs at $\alpha_4 = \alpha_5 = 0$, yield confidence limits that indicate the probability of observing a particular value of α_4 and α_5 based on the $\cos\theta^*_{Jets}$ distribution. The confidence limits used in subsequent sections, 68%, 90% and 99%, are defined using fixed deviations from the minima of χ^2 contours of 2.28, 4.61 and 9.21 respectively. These numbers arise from the integral of the two dimensional χ^2 function.

It proved useful to consider the sensitivities to the individual parameters α_4 and α_5 independently. This was done by projecting out the $\alpha_4 = 0$ or $\alpha_5 = 0$ one dimensional

χ^2 distribution from the two dimensional χ^2 discussed in section 2.4.1. It was then possible to extract the sensitivity to an individual parameters using confidence limits arising from the integral of the one dimensional χ^2 function i.e. 68% confidence limit occurs for $\chi^2 = 0.989$. In subsequent chapters these are the sensitivities quoted for individual anomalous gauge coupling parameters.

2.6.3 Event Weight Interpolation Scheme

As described in section **??**, event weights are used to determine the sensitivity of CLIC to the anomalous gauge couplings. These event weights are extracted on an event by event basis for the signal final state $\nu\nu$qqqq from the generator software Whizard. To achieve a smooth χ^2 distribution a fine sampling of the $\cos\theta^*_{Jets}$ distribution in the α_4 and α_5 space is needed. However, as extracting the event weights is highly CPU intensive, it is unfeasible to produce a finely sampled grid of event weights on an event by event basis by calling the generator. To resolve this issue, an interpolation scheme was applied to determine the event weights within a sampled region of the α_4 and α_5 space. This allows for an infinite sampling of the $\cos\theta^*_{Jets}$ distribution in the space of α_4 and α_5 within the sampled region, without having to call the generator an infinite number of times.

A bicubic interpolation scheme, cubic interpolation along two dimensions, was applied to the event weights that were extracted from the generator. This procedure is best illustrated by showing the interpolated surface superimposed with the raw event weights from the generator, which is shown for several $\nu\nu$qqqq events at 1.4 TeV in figure 2.9. This interpolation scheme produces a smooth and continuous surface that is sufficiently accurate for the fitting procedure applied in this analysis.

For reference at 1.4 TeV event weights were produced from the generator, Whizard, by stepping along α_4 and α_5 in steps of 0.01 ranging from -0.07 to 0.07, as shown in figure 2.2. These range proved to be sufficient for the contours of interest for the CLIC sensitivity analysis at these energies.

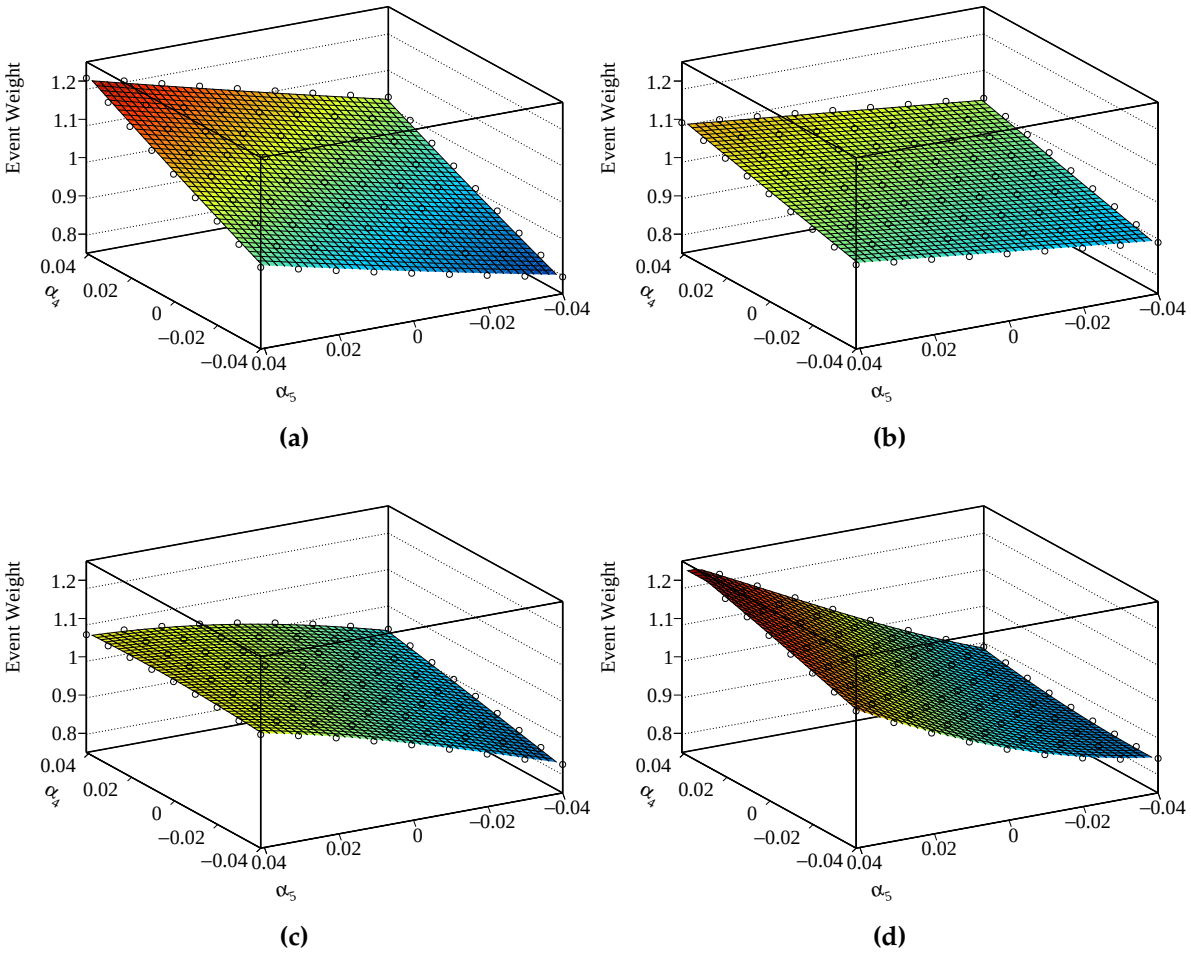

Figure 2.9: A selection of plots showing how the event weight changes when varying the anomalous couplings α_4 and α_5 for 1.4TeV $\nu\nu$qqqq final state events. The hollow circles show the event weight produced from the generator while the surface shown is found using bicubic interpolation between those points.

2.7 Results

The sensitivity of the CLIC experiment to the anomalous gauge couplings α_4 and α_5 at 1.4 TeV is shown in figure 2.10a. This result shows the sensitivity after the application of preselection and MVA described in sections 2.5.1 and 2.5.2 purposed to remove the included background channels, described in section 2.2. These contours yield the one σ confidence limit on the measurement of α_4 to the range -0.00831, 0.0130 and similarly for the measurement of α_5 the range is -0.00606, 0.00904.

2.7.1 Systematic Uncertainties

A source of systematic error in this experiment is the uncertainty on the cross sections for the signal and background final states. Based on the selection efficiencies given in table 2.4, the χ^2 fit procedure is applied on a distribution that primarily consists of the background final states qqqqν arising from the interaction of e^+ and e^+ with beamstrahlung photons. Therefore, uncertainties in the cross section for these backgrounds should be considered. A detailed study of the accuracy of the relevant cross section calculations has yet to be performed for CLIC and so a wide spectrum in the uncertainty of these cross sections is considered here.

This is systematic is included in the χ^2 through the use of a nuisance parameter, whereby the cross section for $\gamma_{BS}e^- \rightarrow$ qqqqν and $e^+\gamma_{BS} \rightarrow$ qqqqν are allowed to fluctuate. Assuming the cross sections are fluctuated by a factor r, the magnitude of the fluctuation is moderated by an additional penalty term in the χ^2 as follows:

$$\chi^2(r) = \sum_i \frac{(O_i - E_i(r))^2}{E_i(r)} + \frac{(r-1)^2}{\sigma_r^2} \tag{2.6}$$

Where O_i is the observed, $\alpha_4 = \alpha_5 = 0$, bin content for bin i in the distribution of $\cos\theta^*_{Jets}$ with no background fluctuations. $E_i(r)$ is the expected, $\alpha_4 \neq 0$ and $\alpha_5 \neq 0$, bin content for bin i in the distribution of $\cos\theta^*_{Jets}$ with the $\gamma_{BS}e^- \rightarrow$ qqqqν and $e^+\gamma_{BS} \rightarrow$ qqqqν background cross sections fluctuated by the factor r. $\sum_i$ is the sum over the bins of the $\cos\theta^*_{Jets}$ distribution. σ_r is the width of the distribution of r, which indicates the uncertainty on the measurement of the fluctuations and hence the background cross sections.

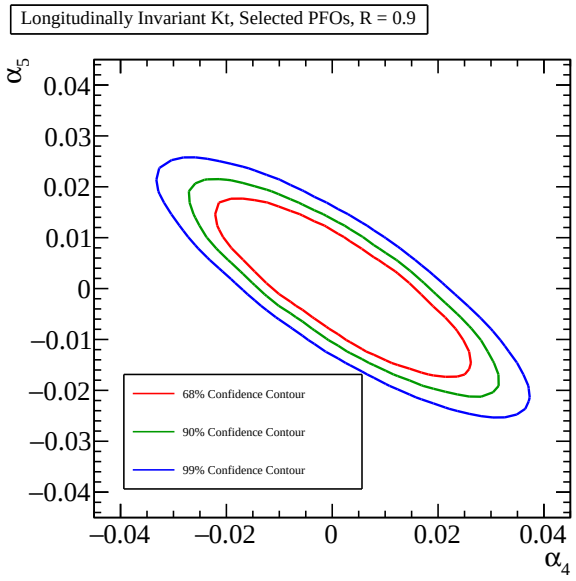

(a) χ^2 sensitivity contours in α_4 and α_5 space.

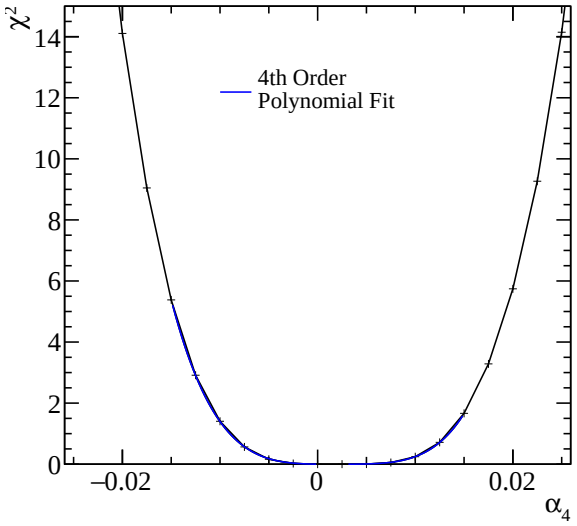

(b) χ^2 as a function of α_4 assuming $\alpha_5 = 0$.

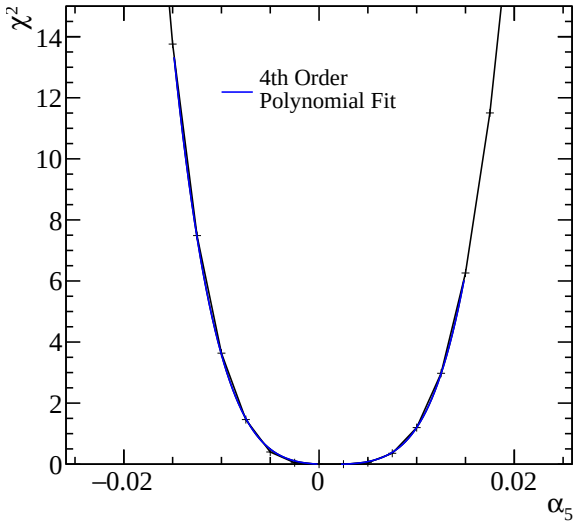

(c) χ^2 as a function of α_5 assuming $\alpha_4 = 0$.

Figure 2.10: χ^2 sensitivity distributions at 1.4 TeV arising from a fit to $\cos\theta^*_{\text{Jets}}$. Results include the effect of backgrounds after the application of preselection and MVA.

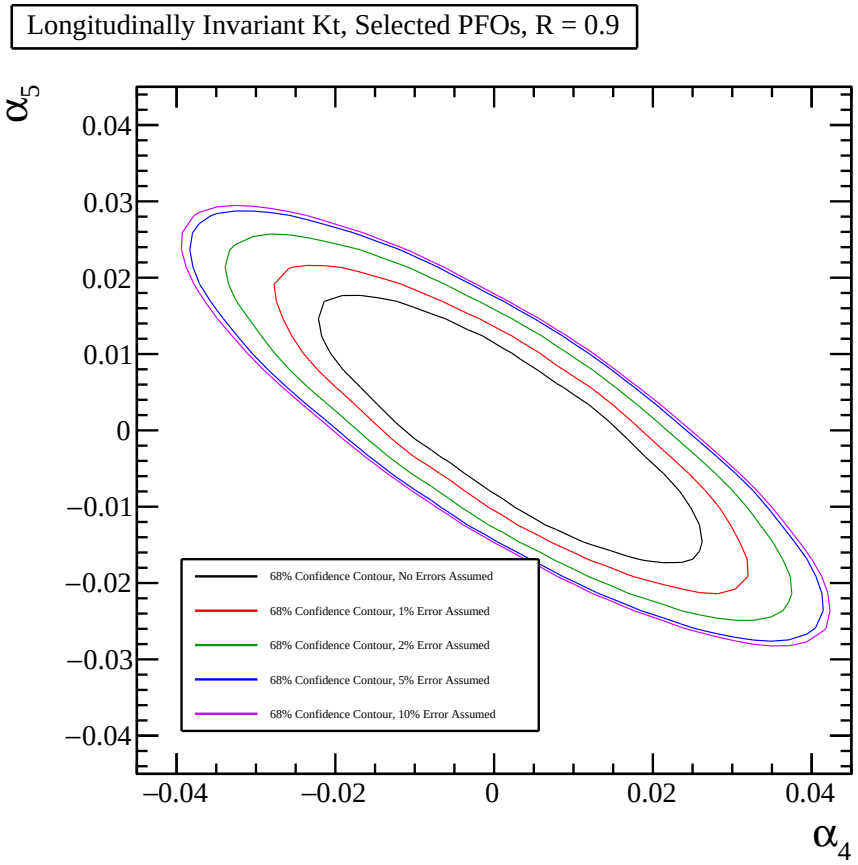

Figure 2.11: 68% sensitivity contour including systematic errors, of varying magnitudes, in dominant background cross sections.

Once again the χ^2 surface is constructed in the space of α_4 and α_5 by minimising $\chi^2(r)$ at each point. The 68% confidence contour is shown with the inclusion of this nuisance parameter for various values of σ_r in figure 2.11.

Minimal changes in sensitivity are observed when allowing the backgrounds to fluctuate beyond the 5% level as the increased luminosity, observed due to the presence of non-zero anomalous gauge couplings, is counteracted by the fluctuations in the backgrounds. In this case shape information in the $\cos\theta^*_{Jets}$ distribution is the only discriminator for the fit. Below the 5% systematic uncertainty level the backgrounds cannot fluctuate enough to overcome the extra luminosity due to the presence of the penalty term.

Based on these contours it is clear that knowledge of the cross section for the $\gamma_{BS}e^- \rightarrow qqqq\nu$ and $e^+\gamma_{BS} \rightarrow qqqq\nu$ backgrounds to sub-percent level is highly desirable for this analysis.

2.8 Sensitivity at 3 TeV

The anomalous gauge coupling sensitivity study described in this chapter was reproduced for CLIC operating at 3 TeV. The procedure for the 3 TeV analysis largely mirrors that of the 1.4 TeV analysis, therefore in this section only the differences between the analyses are highlighted.

The signal and background final states for the 3 TeV analysis were identical to those used for the 1.4 TeV analysis as described in section 2.2. The cross sections at 3 TeV for those signal and background final states can be found in table 2.5. The data analysis and event selection procedures used at 3 TeV mirrored those used at 1.4 TeV. Detailed descriptions of both can be found in sections 2.4 and 2.5 respectively.

Jet finding was performed using the longitudinally invariant k_t algorithm as described in section . Optimisation of the jet algorithm configuration, which uses pure signal only as described in section 2.4.1, found the optimal configuration at 3 TeV to use tight selected PFOs and an R parameter of 1.1. The sensitivity contours and the one dimensional χ^2 distributions for α_4 and α_5, assuming $\alpha_5 = 0$ and $\alpha_4 = 0$ respectively, for the optimal jet configuration at 3 TeV using the $\nu\nu$qqqq signal final state are shown in figure 2.12. Using these distributions the one sigma confidence limits on α_4 is -0.00047 to 0.00048 and on α_5 is -0.00036 to 0.00034.

The event selection for the 3 TeV analysis is summarised in table 2.6.

Due to the increased sensitivity of the signal sample at 3 TeV, the stepping along α_4 and α_5 to extract the event weights from the generator was much finer than was used for the 1.4 TeV analysis. At 3 TeV event weights were taken from the generator in steps of 0.0025 ranging from 0.0045 to -0.0045. Bicubic interpolation was again used to make a continuous surface for the event weights. These event weight surfaces were then used to construct the $\cos\theta^*_{Jets}$ distribution and the χ^2 surface used to determine the reported sensitivities.

The sensitivity of the CLIC experiment to the anomalous gauge couplings α_4 and α_5 at 3 TeV is shown in figure **??**. This result shows the sensitivity after the application of preselection and MVA described in sections 2.5.1 and 2.5.2 purposed to remove the included background channels, described in section 2.2. These contours yield the

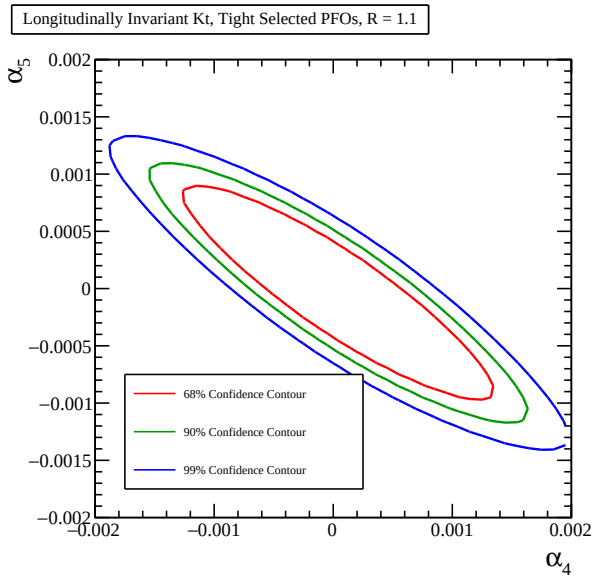

(a) χ^2 sensitivity contours in α_4 and α_5 space.

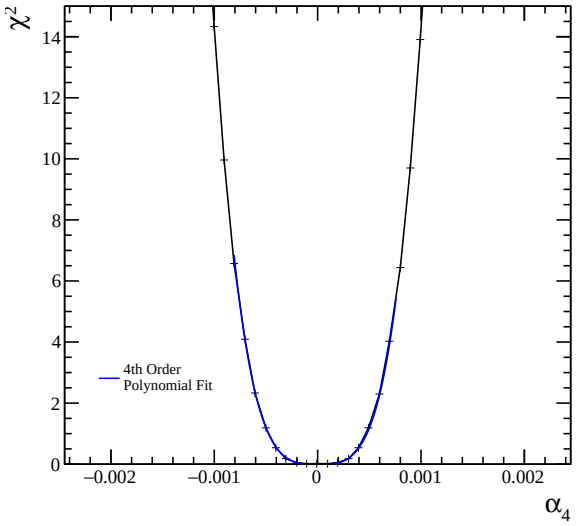

(b) χ^2 as a function of α_4 assuming $\alpha_5 = 0$.

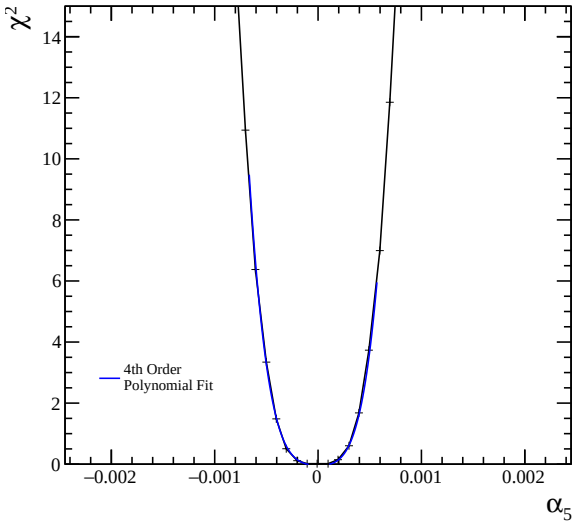

(c) χ^2 as a function of α_5 assuming $\alpha_4 = 0$.

Figure 2.12: χ^2 sensitivity distributions for the qqqq$\nu\nu$ final state arising from a fit to $\cos\theta^*_{\text{Jets}}$ at 3 TeV for the optimal jet reconstruction parameters.

Final State	Cross Section 3 TeV [fb]
$e^+e^- \to \nu\nu qqqq$	71.5
$e^+e^- \to l\nu qqqq$	106.6
$e^+e^- \to llqqqq$	169.3
$e^+e^- \to qqqq$	546.5
$e^+e^- \to \nu\nu qq$	1317.5
$e^+e^- \to l\nu qq$	5560.9
$e^+e^- \to llqq$	3319.6
$e^+e^- \to qq$	2948.9
$\gamma_{EPA}e^- \to qqqqe^-$	287.8
$\gamma_{BS}e^- \to qqqqe^-$	1268.6
$e^+\gamma_{EPA} \to qqqqe^+$	287.8
$e^+\gamma_{BS} \to qqqqe^+$	1267.3
$\gamma_{EPA}e^- \to qqqq\nu$	54.2
$\gamma_{BS}e^- \to qqqq\nu$	262.5
$e^+\gamma_{EPA} \to qqqq\nu$	54.2
$e^+\gamma_{BS} \to qqqq\nu$	262.3
$\gamma_{EPA}\gamma_{EPA} \to qqqq$	402.7
$\gamma_{EPA}\gamma_{BS} \to qqqq$	2423.1
$\gamma_{BS}\gamma_{EPA} \to qqqq$	2420.6
$\gamma_{BS}\gamma_{BS} \to qqqq$	13050.3

Table 2.5: Cross sections of signal and background processes at 3 TeV. In the above table $q \in u$, $\bar{u}$, d, $\bar{d}$, s, $\bar{s}$, c, $\bar{c}$, b or $\bar{b}$ while $l \in e^{\pm}$, $\mu^{\pm}$ or $\tau^{\pm}$ and $\nu \in \nu_e$, ν_μ and ν_τ. The subscript EPA or BS for the incoming photons indicate whether the photon is generated from the equivalent photon approximation or beamstrahlung.

one σ confidence limit on the measurement of α_4 to the range -FILL IN, FILL IN and similarly for the measurement of α_5 the range is -FILL IN, FILL IN.

Final State	ϵ_{presel}	ϵ_{BDT}	N_{BDT}
$e^+e^- \to \nu\nu qqqq$	69.4%	45.3%	64,750
$e^+e^- \to l\nu qqqq$	38.9%	10.9%	23,310
$e^+e^- \to llqqqq$	7.0%	0.7%	2,409
$e^+e^- \to qqqq$	3.4%	0.3%	3,069
$e^+e^- \to \nu\nu qq$	14.4%	0.7%	19,040
$e^+e^- \to l\nu qq$	16.5%	0.3%	27,910
$e^+e^- \to llqq$	0.8%	-	786
$e^+e^- \to qq$	1.1%	-	1,335
$\gamma_{\text{EPA}}e^- \to qqqqe^-$	5.8%	0.5%	2,860
$\gamma_{\text{BS}}e^- \to qqqqe^-$	4.1%	0.4%	8,352
$e^+\gamma_{\text{EPA}} \to qqqqe^+$	5.9%	0.5%	3,063
$e^+\gamma_{\text{BS}} \to qqqqe^+$	4.2%	0.4%	8,090
$\gamma_{\text{EPA}}e^- \to qqqq\nu$	42.8%	16.6%	17,950
$\gamma_{\text{BS}}e^- \to qqqq\nu$	51.6%	26.0%	108,000
$e^+\gamma_{\text{EPA}} \to qqqq\nu$	43.1%	16.6%	17,980
$e^+\gamma_{\text{BS}} \to qqqq\nu$	52.3%	26.5%	109,700
$\gamma_{\text{EPA}}\gamma_{\text{EPA}} \to qqqq$	4.7%	0.4%	3,058
$\gamma_{\text{EPA}}\gamma_{\text{BS}} \to qqqq$	3.0%	0.3%	9,812
$\gamma_{\text{BS}}\gamma_{\text{EPA}} \to qqqq$	3.1%	0.2%	8,880
$\gamma_{\text{BS}}\gamma_{\text{BS}} \to qqqq$	0.6%	-	2,213

Table 2.6: Selection summary at 3 TeV. The subscript EPA or BS for the incoming photons indicate whether the photon is generated from the equivalent photon approximation or beamstrahlung. Cells omitting the efficiency indicate an efficiency of less than 0.1%.

Colophon

This thesis was made in LaTeX 2_ε using the "hepthesis" class [3].

Bibliography

[1] Toshinori Abe et al. The International Large Detector: Letter of Intent. 2010, 1006.3396.

[2] S. Agostinelli et al. GEANT4: A Simulation toolkit. *Nucl. Instrum. Meth.*, A506:250–303, 2003.

[3] Andy Buckley. The hepthesis LaTeX class.

[4] Matteo Cacciari, Gavin P. Salam, and Gregory Soyez. FastJet User Manual. *Eur. Phys. J.*, C72:1896, 2012, 1111.6097.

[5] F. Gaede. Marlin and LCCD: Software tools for the ILC. *Nucl. Instrum. Meth.*, A559:177–180, 2006.

[6] Andreas Hoecker, Peter Speckmayer, Joerg Stelzer, Jan Therhaag, Eckhard von Toerne, and Helge Voss. TMVA: Toolkit for Multivariate Data Analysis. *PoS*, ACAT:040, 2007, physics/0703039.

[7] Wolfgang Kilian, Thorsten Ohl, and Jurgen Reuter. WHIZARD: Simulating Multi-Particle Processes at LHC and ILC. *Eur. Phys. J.*, C71:1742, 2011, 0708.4233.

[8] Lucie Linssen, Akiya Miyamoto, Marcel Stanitzki, and Harry Weerts. Physics and Detectors at CLIC: CLIC Conceptual Design Report. 2012, 1202.5940.

[9] J. S. Marshall, A. MÃijnnich, and M. A. Thomson. Performance of Particle Flow Calorimetry at CLIC. *Nucl. Instrum. Meth.*, A700:153–162, 2013, 1209.4039.

[10] P. Mora de Freitas and H. Videau. Detector simulation with MOKKA / GEANT4: Present and future. In *Linear colliders. Proceedings, International Workshop on physics and experiments with future electron-positron linear colliders, LCWS 2002, Seogwipo, Jeju Island, Korea, August 26-30, 2002*, pages 623–627, 2002.

[11] Mauro Moretti, Thorsten Ohl, and Jurgen Reuter. O'Mega: An Optimizing matrix

element generator. 2001, hep-ph/0102195.

[12] Torbjorn Sjostrand, Stephen Mrenna, and Peter Z. Skands. PYTHIA 6.4 Physics and Manual. *JHEP*, 05:026, 2006, hep-ph/0603175.

[13] M. A. Thomson. Particle Flow Calorimetry and the PandoraPFA Algorithm. *Nucl. Instrum. Meth.*, A611:25–40, 2009, 0907.3577.

[14] Z. Was. TAUOLA the library for tau lepton decay, and KKMC / KORALB / KORALZ /... status report. *Nucl. Phys. Proc. Suppl.*, 98:96–102, 2001, hep-ph/0011305. [,96(2000)].

List of figures

List of tables